

## Bremsstrahlung spectra for Al, Cs, and Au atoms in high-temperature, high-density plasmas

Longhuan Kim, R. H. Pratt, and H. K. Tseng\*

*Department of Physics and Astronomy, University of Pittsburgh, Pittsburgh, Pennsylvania 15260*

(Received 21 January 1985)

Results are presented from a numerical calculation for the bremsstrahlung spectrum and Gaunt factors of Al, Cs, and Au atoms in high-temperature ( $-T$ ), high-density ( $-\rho$ ) plasmas. Plasma temperatures  $kT=0.1$  and  $1.0$  keV and plasma densities  $\rho=\rho_0$  (the normal solid density) and  $\rho=100\rho_0$  are considered. This allows us to determine the generality and identify the origins of features which we had previously identified in calculations for Cs. We also now present results for the total energy loss of an electron in such a plasma. We use a relativistic multipole code which treats the bremsstrahlung process as a single-electron transition in a static screened central potential. We take for the static potential corresponding to an atom in a hot dense plasma the finite-temperature, finite-density Thomas-Fermi model. This approach corresponds to an average atom in local thermodynamic equilibrium. In comparison to isolated-neutral-atom results we observe general suppression of cross sections and a particular suppression in the tip region of the spectrum. Within this model, both superscreening and shape resonances are found in the circumstances of extreme density. At more normal densities and except for the soft-photon end, the spectrum at these energies for an atom in a hot plasma (characterized by an average degree of ionization) can be well represented by the spectrum of the corresponding isolated ion, which has a similar potential shape at the distances which characterize the process.

### I. INTRODUCTION

Bremsstrahlung is one of the basic electron-ion interaction processes. Energetic electron-ion collisions generate x rays whose spectrum provides information regarding both the electrons and the target ions. Bremsstrahlung and inverse bremsstrahlung are among the important mechanisms of thermal transport and energy loss in hot dense plasmas.<sup>1</sup> Bremsstrahlung emission from superthermal electrons in laser-irradiated targets is also a possible diagnostic in laser-target experiments. Several calculations of the bremsstrahlung (free-free) spectrum both for neutral atoms and for ion targets in hot dense plasmas have been reported.<sup>2</sup> Earlier work for bremsstrahlung in these plasmas utilized Born approximation or nonrelativistic dipole approximation in various atomic potential models. Recently,<sup>3</sup> we have reported a full relativistic numerical calculation for electrons of  $1-50$  keV in Cs plasmas of various temperatures and densities, describing the process as a single-electron transition in a screened central potential, making partial wave and multipole expansions and numerically calculating the reduced radial matrix elements over numerically obtained radial wave functions.

This study builds upon our previous work and is intended to determine the generality and identify the origins of the features which were observed. We report the results of calculations for Al and Au plasmas, also identifying some further features of the bremsstrahlung spectrum in hot dense plasmas, including the integrated energy loss of an electron in such a plasma. We use the temperature- and density-dependent Thomas-Fermi (TF) model,<sup>4</sup> obtaining results for the spectrum for plasma densities  $\rho=\rho_0$  to  $100\rho_0$  ( $\rho_0$  the normal solid density) and plasma temperatures  $kT=0.1-1$  keV for incident electron energies

$T_1=1-50$  keV. Our model characterizes the plasma with an average atom in local thermodynamic equilibrium. In order to obtain the spectrum of radiation from the plasma, we would also have to integrate over the distribution of incident electrons, as we have illustrated in our previous work. (In very dense plasmas this would also require taking electron degeneracy into account.) Here, however, our focus is on the elementary processes in the plasma, and the origins of such features as shifts in magnitude with temperature and density, high-energy shape resonances and deep suppression, otherwise of high-frequency radiation.

Our results confirm that most of these features which we obtained in cesium are more general. The varying features of the bremsstrahlung spectrum can generally be understood relatively simply in terms of the corresponding variations in the shape of the atomic potentials. In particular we find that the dependence of the spectrum on plasma temperature and density can be understood from the corresponding variations in the shape of the atomic potentials. Both high temperature and/or high density causes the potential to differ significantly from that of an isolated atom. This affects the spectrum, especially at its soft-photon end, which is more sensitive to the large distance properties of the potential. However, in certain ranges of plasma temperature and density and incident electron energy the spectrum, away from the soft endpoint, can be well represented by that of an isolated ion corresponding to the charge which remains bound in the hot plasma, since these two ionic potentials have the same shape over the range of distances in which the process is determined. However, in very dense plasmas, despite ionization, the spectrum is suppressed below that of the isolated-neutral atom (superscreening), as can be under-

stood from the corresponding superscreened behavior of the potentials. In these circumstances we also find shape resonances at the hard-photon end of the spectrum.

For the cesium plasmas superscreening occurred for  $\rho=100\rho_0$ ,  $kT=0.1$  keV, but not for  $kT=1$  keV. In the Al and Au case, for  $\rho/\rho_0=100$ , superscreening also occurs at high temperature ( $kT=1.0$  keV). Unlike for the cases of Cs and Au plasmas, the comparison of TF spectrum with corresponding ionic spectrum is not appropriate for Al plasmas, since for the temperature and density ranges we consider in this work the TF potential cannot be well represented at short distance by a corresponding ionic potential (for an isolated ion having the same charge as the average ionization number in the plasma).

We begin (Sec. II) with a description of the method of our calculation and the basic assumptions it involves. In Sec. III we describe the atomic potentials we use. Our results for the free-free Gaunt factors in Al, Cs, and Au plasmas are presented in Sec. IV. There we discuss the relationship between the spectrum and the shape of the atomic potential. In Sec. IV we also give our results for the integrated energy loss in these plasmas.

## II. METHOD OF CALCULATION

The theoretical basis of our calculation is the assumption that the bremsstrahlung process may be described as a single-electron transition in a static central potential. Electron wave functions are obtained in a partial-wave series by numerically integrating the radial Dirac equation; a multipole expansion is used for the radiated photon.<sup>5,6</sup> For isolated-neutral atoms, this approach is in good agreement with experiments on the emission of radiation in the scattering of electrons of kinetic energy 1 keV

and above.<sup>7,8</sup> For isolated-neutral atoms we use the relativistic self-consistent Hartree-Fock-Slater potential with local Kohn-Sham exchange (HFS).<sup>9</sup> For the atomic potentials in plasmas we use the finite-temperature, finite-density Thomas-Fermi statistical model.<sup>4</sup> While this is not the best available average-atom model, it is relatively simple and still fairly good. A temperature-density-dependent Hartree-Fock-Slater average-atom model (HSA) has been developed by Rozsnyai.<sup>10</sup> The differences between HSA and TF potentials are fairly small and the results for the bremsstrahlung spectra from these two potentials are similar.<sup>11</sup>

The singly differential cross section, in reduced form  $\sigma \equiv \beta_1^2 Z^{-2} k d\sigma/dk$ , is obtained by evaluating the relativistic matrix element, including retardation,

$$M_{fi} \sim \int \psi_f^* \alpha \cdot \epsilon e^{ik \cdot r} \psi_i d^3r. \quad (1)$$

Here  $k$  is the photon energy,  $Z$  the nuclear charge of the target, and  $\beta_1 \equiv v_1/c$  the reduced velocity of the incident electron. This approach omits higher-order electrodynamic effects, multiphoton processes, exchange, correlation, and excitation effects among atomic electrons. The free-free Gaunt factor  $g(T_1, k/T_1)$  is defined for given incident electron kinetic energy  $T_1$  and  $k$  as the ratio between the reduced cross section  $\sigma$  and the corresponding semiclassical result  $\sigma_{cl}$  given by Kramers:

$$g = \sigma / \sigma_{cl}, \quad (2)$$

where  $\sigma_{cl} = 5.61$  mb.

The radiative energy loss in scattering, for electrons with a given incident kinetic energy  $T_1$ , can be obtained by integrating  $kd\sigma/dk$  over all photon energies  $k$  from 0 to  $T_1$ . The energy loss of an electron per unit path length is

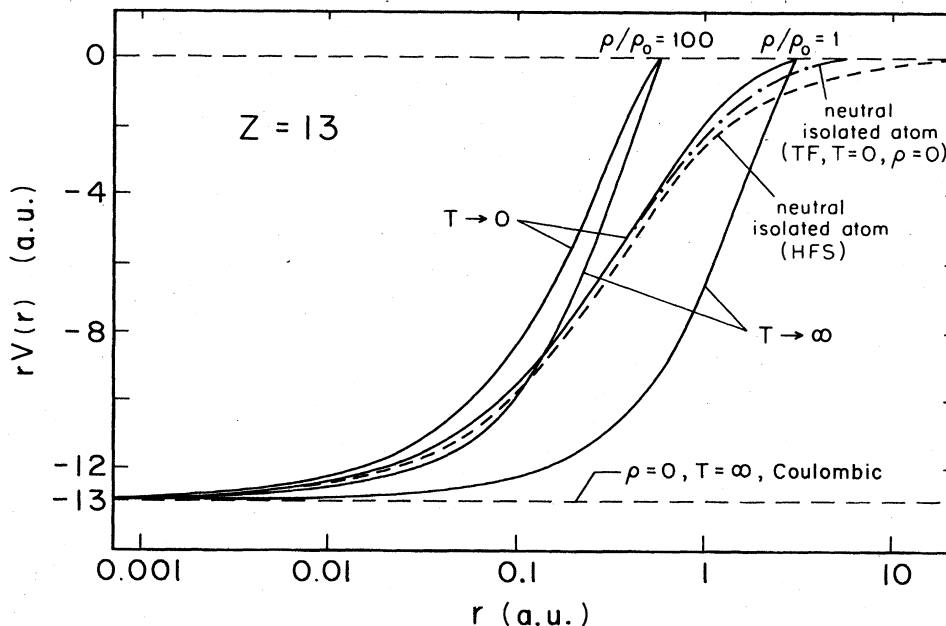


FIG. 1. Comparison of TF potential with  $T \rightarrow 0$  and  $T \rightarrow \infty$  limits for low and high plasma densities.

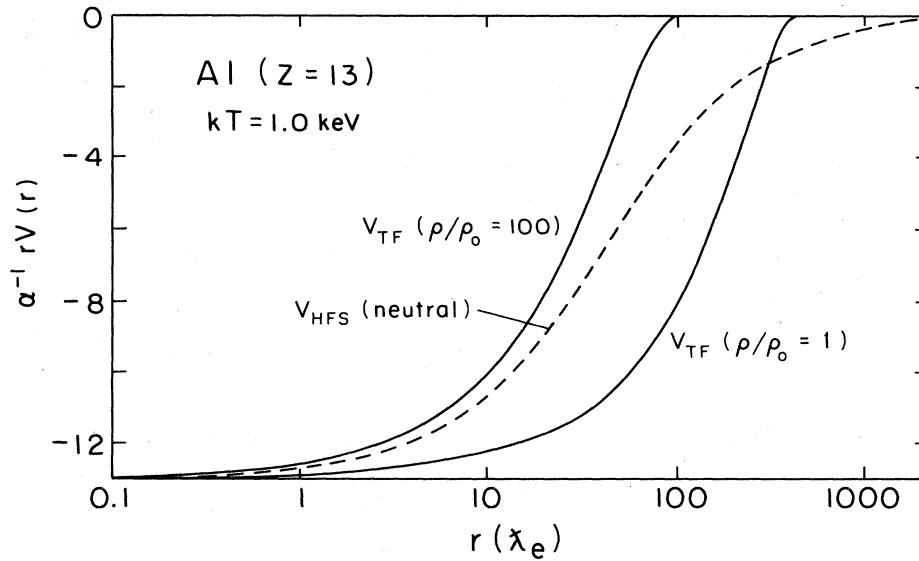


FIG. 2. Comparison of TF potential with isolated-atom or -ion potentials for Al ( $Z=13$ ), plasma density  $\rho/\rho_0=1$  and 100; plasma temperature  $kT=1$  keV. We plot  $rV$  which goes to  $Z=13$  for  $r=0$  and to 0 (neutral case) or the ionic charge for large distances.

$$\begin{aligned} -dE/dx &= N \int_0^{T_1} k(d\sigma/dk)dk \\ &= NZ^2\beta_1^{-2}T_1\sigma_{cl} \int_0^1 g(T_1, k/T_1)d(k/T_1), \end{aligned} \quad (3)$$

integrated over the spectrum for fixed  $T_1$ , where  $N$  is the number of atoms per unit volume,  $Z$  is the atomic number of the target atom,  $\beta_1 \equiv v_1/c$ ,  $c$  is the velocity of light,  $T_1$  is the kinetic energy of the incident electron, and  $g(T_1, k/T_1)$  is the Gaunt factor. The integrated energy loss  $\mathcal{E}_{loss}$  is defined by<sup>6</sup>

$$\begin{aligned} \mathcal{E}_{loss} &\equiv Z^{-2}\alpha^{-3}\lambda_e^{-2}E^{-1} \int_0^{T_1} (k d\sigma/dk)dk \\ &= (T_1/E)\beta_1^{-2}\alpha^{-3}\lambda_e^{-2}\sigma_{cl} \int_0^1 g(T_1, k/T_1)d(k/T_1), \end{aligned} \quad (4)$$

so that

$$-dE/dx = NZ^2\alpha^3\lambda_e^2\mathcal{E}_{loss}E, \quad (5)$$

where  $\lambda_e$  is the electron Compton wavelength,  $\alpha=1/137.036$ , and  $E$  is the total energy (including rest-mass energy) of the incident electron.

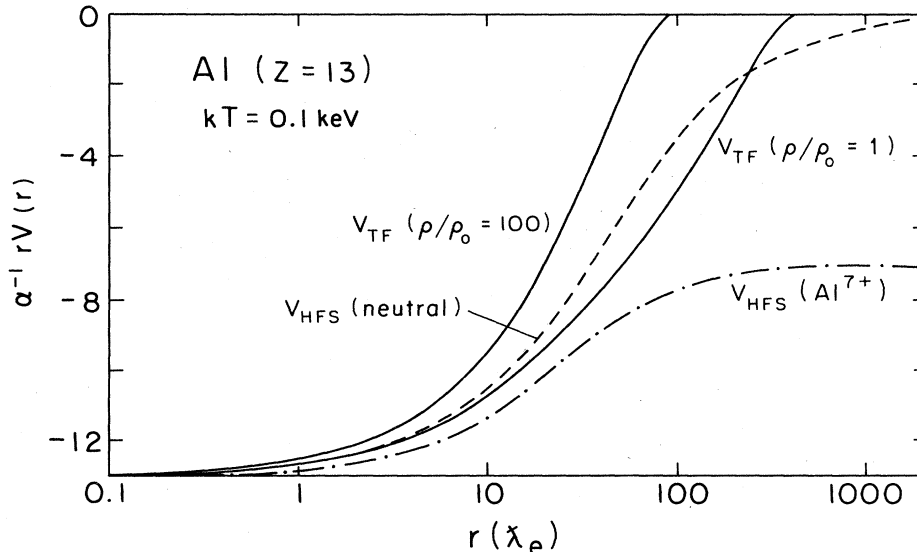
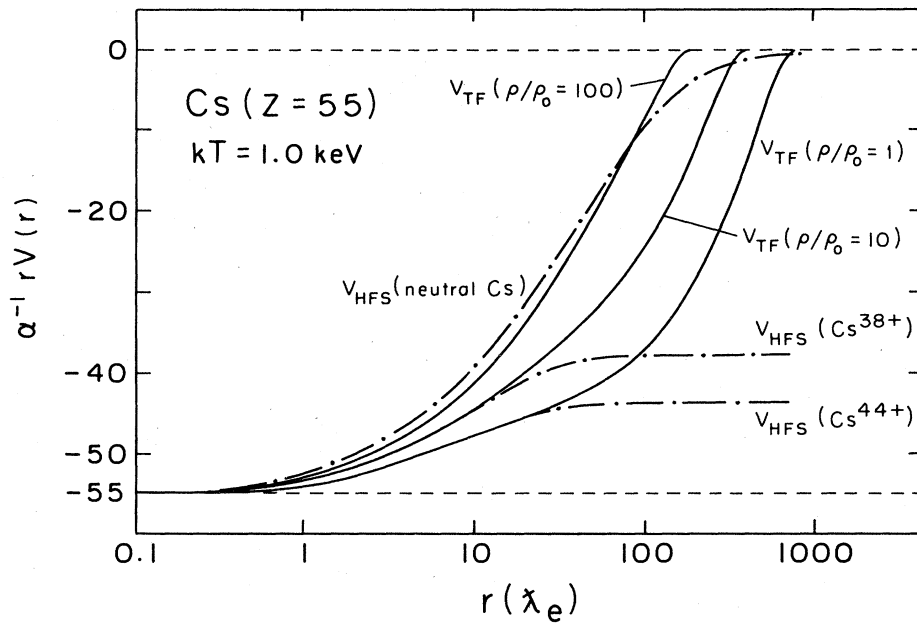


FIG. 3. Same as Fig. 2, but for  $kT=0.1$  keV.

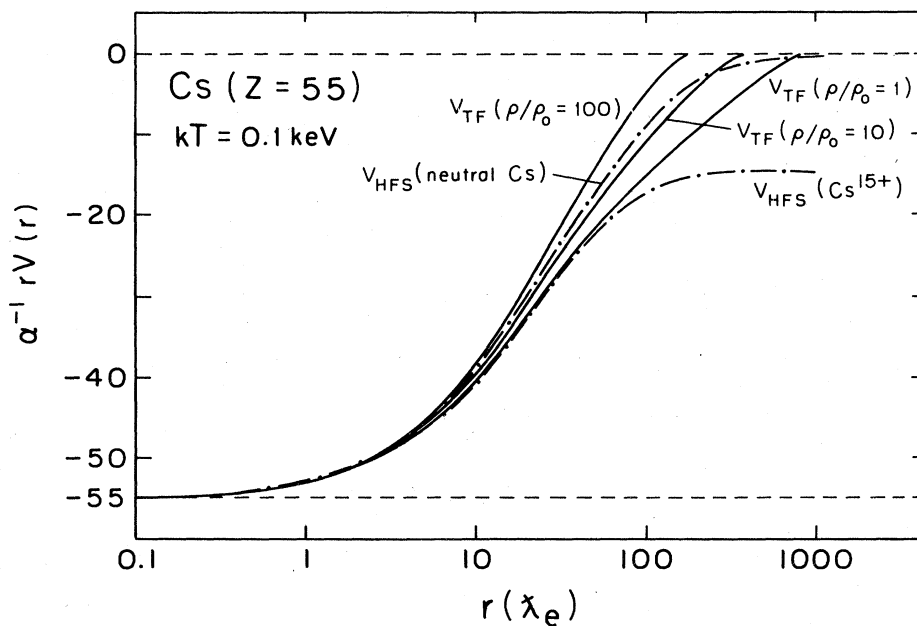
FIG. 4. Same as Fig. 2, but for Cs ( $Z = 55$ ).

### III. RESULTS FOR ATOMIC POTENTIALS

The finite-temperature, finite-density Thomas-Fermi model describes an atom as a sphere containing the nucleus at its center and bound and continuum electrons inside its finite volume. For an atom in a dense plasma the radius  $r_a$  of the atomic sphere is determined in terms of the density of the plasma as  $r_a = (4\pi n_i/3)^{-1/3}$ , where  $n_i$  is the ion number density. Due to screening by bound and free electrons the TF potential vanishes at the atom

boundary. Isolated-neutral-atom potentials become zero only at infinity.

To understand the general behavior of the TF potential, we begin by showing in Fig. 1 the TF potential (for  $Z = 13$ ) at densities  $\rho = 0$ ,  $\rho = \rho_0$ , and  $\rho = 100\rho_0$  ( $\rho_0$  is normal solid density) in both the  $T = \infty$  and  $T = 0$  limits. For the isolated-neutral-atom case ( $T = 0$ ,  $\rho = 0$ ) we have also shown the self-consistent Hartree-Fock-Slater (HFS) potential. We plot  $rV(r)$ , which approaches  $-Z$  for  $r = 0$  and reduced to zero at a finite distance (finite-

FIG. 5. Same as Fig. 4, but for  $kT = 0.1$  keV.

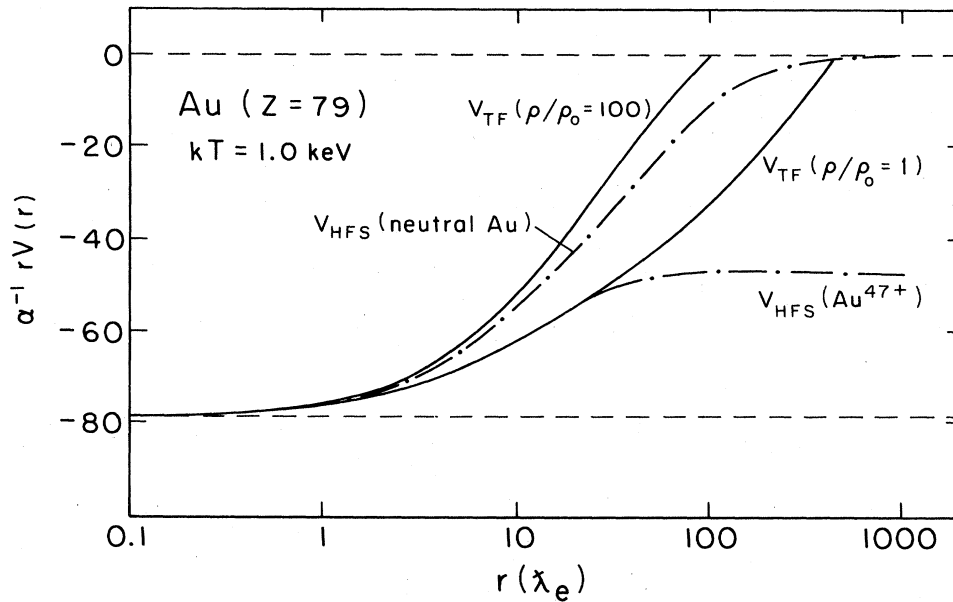


FIG. 6. Same as Fig. 2, but for Au ( $Z=79$ ).

density case) or infinity (isolated-neutral-atom case). For the Coulomb potential the curve is a horizontal line, as shown in Fig. 1. For the high densities considered here the differences from isolated-neutral atoms, due to the cutoff of the potential at finite distances, are significant. For a fixed plasma density, with increasing temperature the potential becomes somewhat more Coulombic (horizontal line), approaching in the high-temperature limit that of a positive point charge imbedded in a uniform neutralizing negative-charge distribution.

In Figs. 2–7 we show comparisons of TF potentials

with corresponding isolated-neutral-atom and -ion potentials for Al, Cs, and Au, for plasma densities  $\rho=\rho_0$  and  $\rho=100\rho_0$ , plasma temperature  $kT=0.1$  and 1 keV. The degree of ionization  $Z^*$  is specified as  $Z^*=Zn_e(r_a)/\langle n_e \rangle$ , where  $\langle n_e \rangle \equiv Zn_i$  is the average electron density and  $n_e(r_a)$  is the electron density at the atom boundary. The values of  $Z^*$  calculated within the TF model are shown in Table I. Note that at low temperature, ionization is increasing with density (pressure ionization) while at high temperature it is decreasing.

It is interesting to compare these TF potentials with

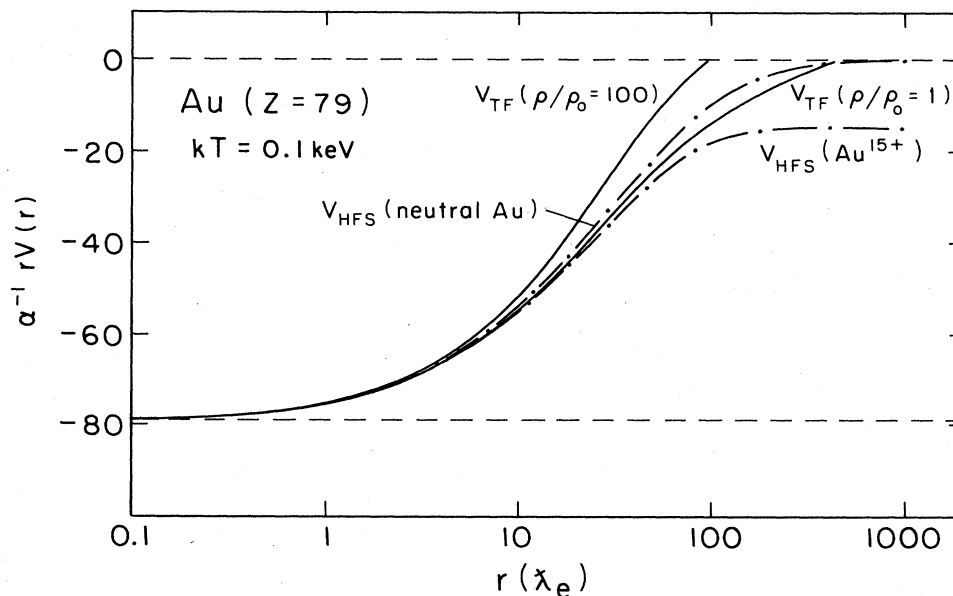


FIG. 7. Same as Fig. 6, but for  $kT=0.1$  keV.

TABLE I. Average ionization  $Z^*$  of  $^{13}\text{Al}$ ,  $^{55}\text{Cs}$ , and  $^{79}\text{Au}$  atoms for various plasma temperatures and densities according to the Thomas-Fermi statistical model, with the definition  $Z^* = Zn_e(r_a)/\langle n_e \rangle$ , where  $r_a$  is the atom-boundary radius,  $n_e(r_a)$  is the electron number density, and  $\langle n_e \rangle$  is the electron density averaged over the atomic volume.

	$kT=0.1$ keV		$kT=1.0$ keV	
	$\rho/\rho_0=1$	$\rho/\rho_0=100$	$\rho/\rho_0=1$	$\rho/\rho_0=100$
$^{13}\text{Al}$	$Z^*=7$	$Z^*=8.7$	$Z^*=12.3$	$Z^*=10.7$
$^{55}\text{Cs}$	$Z^*=15$	$Z^*=18$	$Z^*=44$	$Z^*=33$
$^{79}\text{Au}$	$Z^*=15$	$Z^*=37.6$	$Z^*=47$	$Z^*=41.9$

corresponding isolated ionic potentials of the same  $Z^*$ , which we have calculated within the self-consistent HFS model. For Cs ( $Z=55$ ) and Au ( $Z=79$ ) with  $\rho=\rho_0$  we find that in the interior of the atom, particularly near the atomic nucleus, the finite-temperature, finite-density TF potentials are very close to the corresponding potentials for isolated ions of the same  $Z^*$ . However, at higher density the potential is closer to that of an isolated neutral atom than its degree of ionization would suggest, while at high enough density and low temperature the TF potential is even less attractive than in the neutral case (super-screening). The atom has been pressure rather than temperature ionized; the continuum electrons are confined to a small volume and more completely screen the nucleus than the corresponding bound electrons in the isolated neutral case. Note this feature is always present near the boundary of a confined atom, but in the superscreening case it occurs throughout much of the interior of the atom as well.

#### IV. RESULTS FOR FREE-FREE SPECTRA

Figures 8–15 show our results for the Gaunt factors of electron bremsstrahlung for Al, Cs, and Au plasmas at densities  $\rho/\rho_0=1$  and 100, and temperatures  $kT=0.1$  and 1 keV. Isolated-neutral-atom and isolated-ion results are also illustrated in Figs. 8–15. Due to their long-range Coulombic behavior, the ionic spectra diverge logarithmically at the soft-photon endpoint. (Note there are some revisions in the curves taken from Ref. 3. The ionic spectra in Figs. 3 and 4 of Ref. 3 were not accurate in the soft-photon region. Also there was an error in one of the TF spectra in Fig. 5 of Ref. 3.)

We see that for  $\rho/\rho_0=1$  in the Cs and Au cases (Figs. 10, 11, 13, 14), in the large portion of the spectrum ( $k/T_1 \gtrsim 0.4$ ) the Gaunt factors  $g^{\text{TF}}$  calculated from the TF potential are very close to  $g(Z^*)$ , the Gaunt factor of the isolated ion of corresponding degree of ionization. This occurs because, in the hard-photon region of the spectrum, the bremsstrahlung process at these energies is determined at relatively small distances, where the TF potential and the corresponding ionic potential are similar, as discussed in Sec. III.

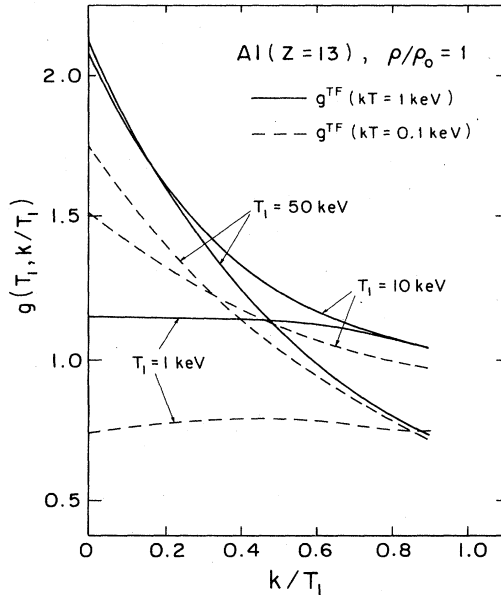


FIG. 8. Free-free Gaunt factors obtained by full relativistic calculation in the TF potential ( $g^{\text{TF}}$ ), as a function of  $k/T_1$  (ratio of photon energy radiated to incident electron kinetic energy) for Al plasmas at  $kT=0.1$  and 1 keV,  $\rho/\rho_0=1$ , for incident electron energies  $T_1=1, 10$ , and 50 keV, compared with isolated-neutral-atom results.

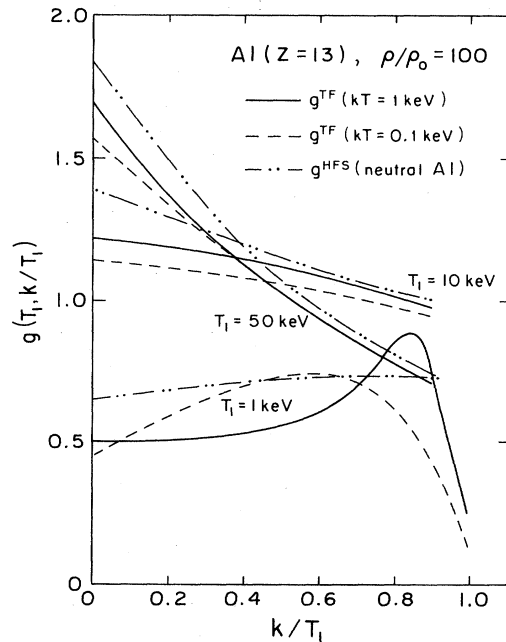


FIG. 9. Same as Fig. 8, but  $\rho/\rho_0=100$ .

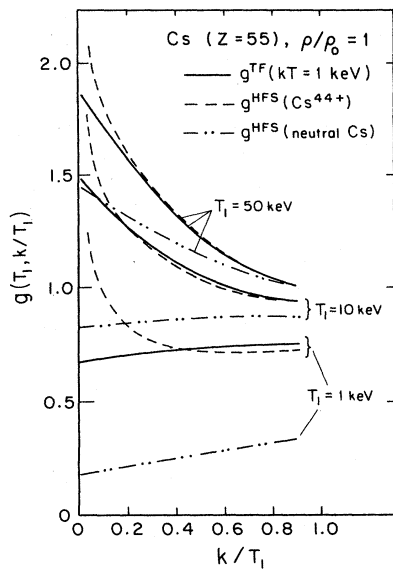


FIG. 10. Same as Fig. 8, but for Cs ( $Z=55$ ) plasma and  $kT=1$  keV,  $\rho/\rho_0=1$ , and also including ion ( $\text{Cs}^{44+}$ ) results.

For a given plasma and given incident electron energy, the higher the temperature the larger the Gaunt factors; also in these circumstances the higher the density the smaller the Gaunt factors. These features are understandable since higher temperature or lower density gives less screened potentials and hence larger cross sections. At very high density and low temperature ( $\rho=100\rho_0$ ,  $kT=0.1$  keV), the TF potentials can be more screened than in the neutral atom (Figs. 2, 3, 5–7). We see (Figs. 9, 12, 15) that the Gaunt factors for these plasmas lie below the neutral-atom curves. For the Al and Au plasmas this occurs even for  $kT=1$  keV, while for cesium, the spectrum for  $\rho/\rho_0=100$ ,  $kT=1$  keV is slightly above

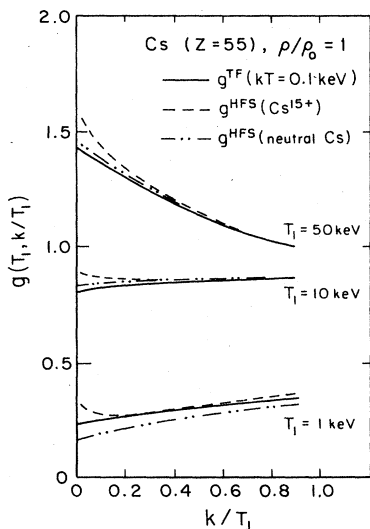


FIG. 11. Same as Fig. 10, but for  $kT=0.1$  keV, and compared with  $\text{Cs}^{15+}$  ion results.

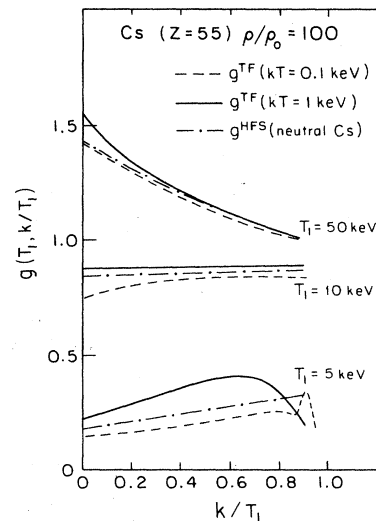


FIG. 12. Same as Fig. 10, but for  $\rho/\rho_0=100$ ,  $kT=0.1$  and 1 keV, compared with neutral-atom results.

the neutral-atom curve. We understand this difference in Cs by noting that  $\rho/\rho_0=100$  means less free-electron confinement for cesium than for aluminum and gold. The normal density  $\rho_0$  of cesium is much less than for Al and Au ( $\rho_0=1.89$  gm/cm<sup>3</sup> for Cs;  $\rho_0=2.79$  m/cm<sup>3</sup> for Al;  $\rho_0=19.39$  m/cm<sup>3</sup> for Au), while the atomic weight is relatively high (133 for Cs; 27 for Al, 197 for Au). Consequently, the atomic radius  $r_a$  for Cs in the case  $\rho/\rho_0=100$  is much larger than for Al and Au (in atomic units,  $r_a=1.23$  for Cs,  $r_a=0.64$  for Al, and  $r_a=0.65$  for Au).

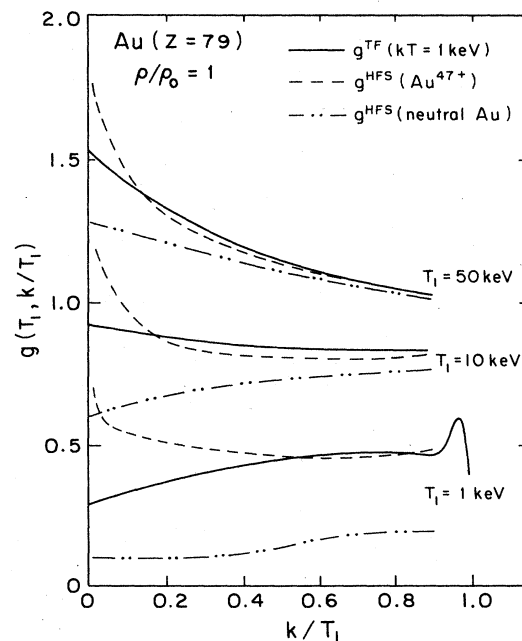


FIG. 13. Same as Fig. 8, but for Au ( $Z=79$ ),  $kT=1$  keV,  $\rho/\rho_0=1$ , compared with  $\text{Au}^{47+}$  results.

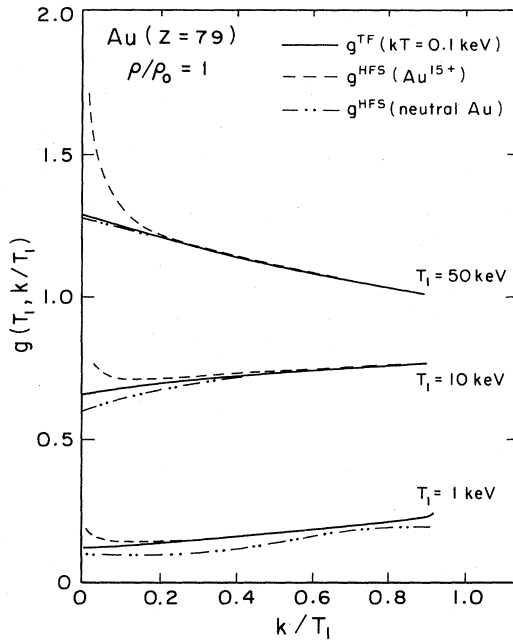


FIG. 14. Same as Fig. 13, but for  $kT=0.1$  keV, compared with  $\text{Au}^{15+}$  results.

This density for Cs is not high enough to overcome the temperature ionization effects for  $kT=1$  keV. To test this understanding, we tried a higher density for Cs which corresponds to a comparable atomic radius ( $\rho=1000\rho_0=1890$  gm/cm<sup>3</sup>,  $kT=1$  keV,  $r_a=0.57$  a.u.,  $T_1=10$  keV) and indeed found that the gaunt factors are

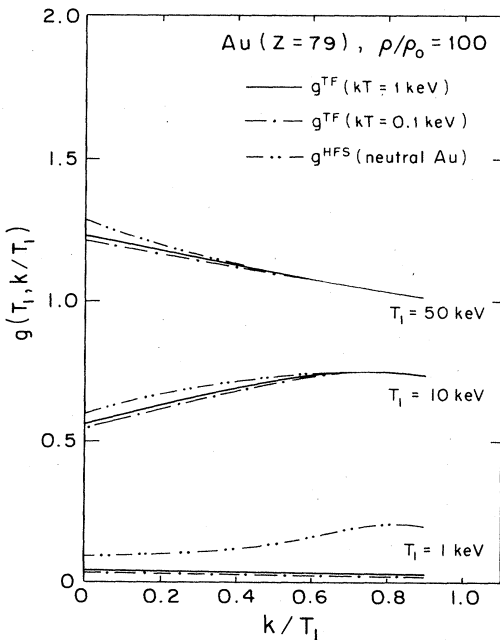


FIG. 15. Same as Fig. 13, but for  $\rho/\rho_0=100$ ,  $kT=0.1$  and 1 keV.

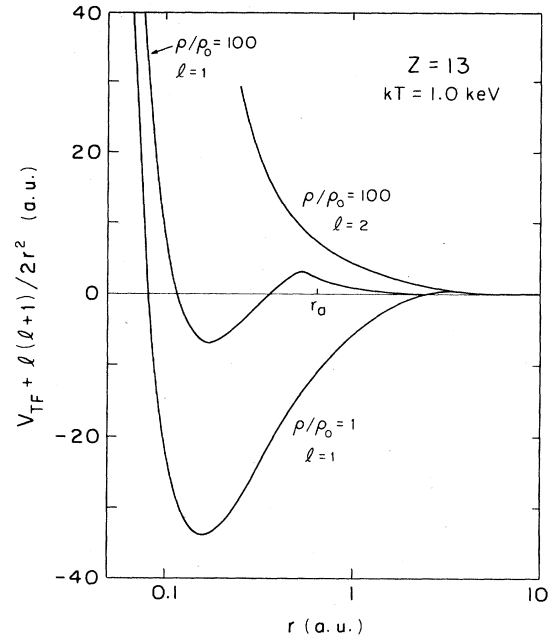


FIG. 16. Effective potential  $V_{\text{eff}}=V_{\text{TF}}+l(l+1)/(2r^2)$  for an incident electron with angular momentum  $l=1$  and 2 in an aluminum plasma of  $kT=1$  keV,  $\rho/\rho_0=1$  and 100.

lower than those of the isolated-neutral atom.

Another important feature in the high-density free-free spectra is the presence of shape resonances (Figs. 9, 12, 15). In our calculations we see shape resonances near the hard-photon endpoint for low-electron incident energy ( $T_1=1$  keV) at high plasma density ( $\rho/\rho_0=100$ ) and various temperatures ( $kT=1$  keV for Al and Au;  $kT=0.1$  keV for Cs). These resonances occur for outgoing continuum electron kinetic energies of about 100 eV. Such resonances occur in our model because of the sharp cutoff of the screened potential at relatively short distances due to the small atomic boundary at high density, where the centrifugal potential which extends beyond the atom boundary is still quite large. (It is not clear how seriously we should take this feature of our model.) In Fig. 16 we illustrate in Al the effective potentials  $V_{\text{eff}}$  for angular momentum  $l=1$  and  $l=2$ , where  $V_{\text{eff}}=V_{\text{TF}}+l(l+1)/(2r^2)$  and  $V_{\text{TF}}$  is the static atomic potential given by the TF model. We see in this case that, for the high density  $\rho=100\rho_0$ , the effective potential with  $l=1$  has a high barrier near the atomic edge, while for the low density  $\rho=\rho_0$  the barrier is much smaller. Hence for a low-density plasma, as in the isolated-neutral-atom cases, shape resonances in the spectrum occur only when the final electron energy is in the few-eV range,<sup>12</sup> while at high density, resonances can occur for larger final energies. At higher energies, higher angular momentum final states are more important in cross section and so also larger magnitude shape-resonance effects occur in these processes.

We also notice, in addition to the shape resonance, another unusual feature of the spectra at high density. The  $T_1=1$  keV curves of Al and Cs show great suppres-

TABLE II. Results of energy-loss calculation for  $^{13}\text{Al}$ ,  $^{55}\text{Cs}$ , and  $^{79}\text{Au}$  plasmas. Here  $T_1$  is the incident electron kinetic energy. Numbers shown are the integrated energy losses  $\mathcal{E}_{\text{loss}} \equiv Z^{-2} \alpha^{-3} \lambda_e^{-2} E^{-1} \times \int_0^{T_1} (kd\sigma/dk) dk$ . TF, Thomas-Fermi model, with  $kT$  the plasma temperature in keV;  $\rho$ , the plasma density;  $\rho_0$ , normal solid density of the element. ION, isolated-ion model. INA, isolated-neutral-atom model. The two ion models for Cs and Au correspond to the average ionization at density  $\rho = \rho_0$  for the two plasma temperatures in Cs ( $kT = 1.0$  keV with  $^{55}\text{Cs}^{44+}$  and  $kT = 0.1$  keV with  $^{55}\text{Cs}^{15+}$ ), and similarly in Au.

		$T_1 = 50$ keV	$T_1 = 10$ keV	$kT_1 = 1$ keV
$^{13}\text{Al}$	TF ( $kT = 1.0$ , $\rho = \rho_0$ )	6.15	6.62	5.40
	TF ( $kT = 0.1$ , $\rho = \rho_0$ )	5.60	5.71	3.75
	TF ( $kT = 1.0$ , $\rho = 100\rho_0$ )	5.45	5.38	2.78
	TF ( $kT = 0.1$ , $\rho = 100\rho_0$ )	5.36	5.12	2.82
	INA	5.81	5.80	3.45
$^{55}\text{Cs}$	TF ( $kT = 1.0$ , $\rho = \rho_0$ )	6.56	5.41	3.53
	TF ( $kT = 0.1$ , $\rho = \rho_0$ )	5.94	4.19	1.51
	TF ( $kT = 1.0$ , $\rho = 100\rho_0$ )	5.90	4.40	1.50
	TF ( $kT = 0.1$ , $\rho = 100\rho_0$ )	5.91	4.06	1.03
	ION ( $\text{Cs}^{44+}$ )	6.88	5.62	4.04
	ION ( $\text{Cs}^{15+}$ )	6.06	4.30	1.58
INA	5.94	4.15	1.19	
$^{79}\text{Au}$	TF ( $kT = 1.0$ , $\rho = \rho_0$ )	6.04	4.16	2.09
	TF ( $kT = 0.1$ , $\rho = \rho_0$ )	5.67	3.57	0.88
	TF ( $kT = 1.0$ , $\rho = 100\rho_0$ )	5.57	3.37	0.17
	TF ( $kT = 0.1$ , $\rho = 100\rho_0$ )	5.55	3.32	0.13
	ION ( $\text{Au}^{47+}$ )	6.08	4.30	2.55
	ION ( $\text{Au}^{15+}$ )	5.73	3.60	0.98
	INA	5.71	3.53	0.77

sion at the hard-photon endpoint (see Figs. 9 and 13), which has not been seen in neutral-atom or ion cases. This results from a reduced normalization (small-distance magnitude) of outgoing electron continuum waves, which do not penetrate through the more compact screening into the interior attractive nuclear charge. For the less compact isolated-neutral-atom case, only in the last tens of eV will the spectrum start dropping as low-energy screened-continuum normalizations begin to differ substantially from Coulomb.

In Table II we give the results of energy-loss calculations for Al, Cs, and Au plasmas. Results from corresponding isolated ions and atoms are also presented for comparison. Due to the logarithmic divergence of the ionic spectra at the soft-photon endpoint and the difficulty of partial wave calculations for the soft-photon region, which is more easily estimated via the low-energy theorem, exact numerical partial wave calculation is not appropriate in ions for these regions. We use the simple parametrization of bremsstrahlung spectra for isolated ions and atoms, developed by Feng and Pratt,<sup>13</sup> to generate values of spectra in these regions. The results shown

for neutral atoms are obtained from Ref. 6. In spite of the logarithmic divergence of the spectra at the soft-photon endpoint the integrated energy loss obtained from ion spectra is close to that from corresponding normal density TF spectra, and closer than neutral-atom results in most cases. For the particular higher-density and lower-temperature situations considered here ( $\rho = 100\rho_0$ ,  $kT = 0.1$  keV) the neutral-atom results are adequate, as one would expect from a comparison of the spectra. Generally, the energy losses calculated from TF, isolated-ion and isolated-atom potentials are less different for higher incident electron energy than for lower incident energy. At low energy the spectra depend more on the potential at long distance, where the models differ more from each other.

#### ACKNOWLEDGMENTS

One of the authors (L.K.) wishes to thank M. Lamoureux for helpful discussions. This work is supported in part by the U.S. National Science Foundation under Grant No. PHY-81-20785.

\*Permanent address: Department of Physics, National Central University, Chung-li, Taiwan, Republic of China.

<sup>1</sup>For a review, see R. M. More, in *Applied Collision Physics*, edited by C. J. Barnett (Academic, New York, 1984), Vol. II.

<sup>2</sup>For a list of such work see Ref. 3.

<sup>3</sup>I. J. Feng, M. Lamoureux, R. H. Pratt, and H. K. Tseng, *Phys. Rev. A* **27**, 3209 (1983).

<sup>4</sup>R. Feynman, N. Metropolis, and E. Teller, *Phys. Rev.* **75**, 1561

- (1949).
- <sup>5</sup>H. K. Tseng and R. H. Pratt, *Phys. Rev. A* **3**, 100 (1971).
- <sup>6</sup>R. H. Pratt, H. K. Tseng, C. M. Lee, Lynn Kissel, Crawford MacCallum, and Merle Riley, *At. Data Nucl. Data Tables* **20**, 175 (1977); **26**, 477(E) (1981).
- <sup>7</sup>M. Semaan and C. Quarles, *Phys. Rev. A* **26**, 3152 (1982).
- <sup>8</sup>C. M. Lee, Lynn Kissel, and R. H. Pratt, *Phys. Rev. A* **13**, 1714 (1976).
- <sup>9</sup>D. A. Liberman, D. T. Cromer, and J. T. Walker, *Comput. Phys. Commun.* **2**, 107 (1971).
- <sup>10</sup>B. F. Rozsnyai, *Phys. Rev. A* **5**, 1137 (1972).
- <sup>11</sup>M. Lamoureux, I. J. Feng, R. H. Pratt, and H. K. Tseng, *J. Quant. Spectrosc. Radiat. Transfer* **27**, 227 (1982).
- <sup>12</sup>C. M. Lee and R. H. Pratt, *Phys. Rev. A* **12**, 707 (1975).
- <sup>13</sup>I. J. Feng and R. H. Pratt, University of Pittsburgh Report No. PITT-266 (unpublished).